ELSEVIER

Polymer 43 (2002) 2451–2465

polymer

www.elsevier.com/locate/polymer

Hot-drawing of poly(methyl methacrylate) and simulation using a glass–rubber constitutive model

P.J. Dooling[a,1], C.P. Buckley[a,*], S. Rostami[b], N. Zahlan[b]

[a]*Department of Engineering Science, University of Oxford, Parks Road, Oxford OX1 3PJ, UK*
[b]*ICI plc, Wilton Centre, Middlesbrough, Cleveland TS90 8JE, UK*

Received 10 July 2001; received in revised form 10 November 2001; accepted 28 November 2001

Abstract

The large-deformation three-dimensional glass–rubber constitutive model for isotropic, amorphous, linear polymers near the glass transition, previously proposed, has been extended to include a spectrum of network relaxations. In addition, an experimental programme of uniaxial tension and compression tests was carried out on high molecular weight cast sheets of poly(methyl methacrylate) (PMMA), with varying strain-rate and temperature across the range from 114 to 190 °C, encompassing the thermoforming range of practical importance. The extended model was found to fit successfully the data for PMMA, provided a doublet network relaxation spectrum was employed. The original model, with only a single network relaxation, was found to be grossly inadequate when there was significant network relaxation by entanglement slippage. Parameters of the model for PMMA, obtained by fitting to the new data, were compared with values obtained by other routes.

Keywords: Constitutive model; Poly(methyl methacrylate); Hot-drawing

1. Introduction

In some important manufacturing processes, amorphous thermoplastic polymers undergo large stretching flows above the glass transition. Examples are thermoforming, biaxial stretching of films, and bottle blowing. In the optimisation of these processes, and of the materials for them, it is clearly desirable to be able to carry out numerical simulations of them, for example by exploiting the finite element (FE) method. At present, however, the FE analyst faces a major problem: polymers show complex constitutive response in the relevant ranges of temperature and rate. As usual, the engineering need is for a constitutive model that captures the essential features of material behaviour, but *at low computational cost*. The latter point is crucial. To be useful, FE analyses must not be too slow. The aim of the work described here was to devise a suitable constitutive model, for use in simulating hot-stretching of cast sheets of uncrosslinked poly(methyl methacrylate) (PMMA), in the temperature range immediately above the glass transition, such as encountered in thermoforming or biaxial orientation processes.

The complexity of response results from the fact that, under these conditions, the polymer is highly dependent on rate and temperature. It exhibits features associated with several physical processes, best described in terms of the 'tube' model for linear polymers [1]. Their relative dominance is a sensitive function of rate and temperature. At the highest rates and lowest temperatures, close to the glass transition, the stress tensor is dominated by the contribution due to stretching of primary and secondary bonds σ^b, relaxed by segmental motion within the tube (longest time constant = the Rouse time τ_e for motion on a length scale of up to one tube diameter). The response is that of a viscoelastic glassy solid. In the intermediate region, the stress is dominated by that arising from conformational entropy reduction σ^c, as molecules are constrained to follow the stretch of the tube. The response is that of a hyperelastic rubbery solid. At the lowest rates and highest temperatures the conformational stress relaxes, first by retraction along the tube (time constant = the Rouse time τ_R for motion on a length scale of the whole molecule) and finally by escape from the tube (time constant = the disengagement or 'reptation' time τ_d). The response is that of an elastoviscous fluid.

The last two decades have seen great strides in

* Corresponding author. Tel.: +44-1865-273156; fax: +44-1865-273906.
E-mail address: paul.buckley@eng.ox.ac.uk (C.P. Buckley).
[1] Present address: ICI plc, Wilton Centre, Middlesbrough, Cleveland TS90 8JE, UK.

0032-3861/02/$ - see front matter
PII: S0032-3861(01)00799-6

constructing a molecular theory of the above sequence of processes in terms of the tube model—for a recent review see McLeish and Milner [2]. But the molecular theory per se does not yet provide a viable model for the present context. Firstly, certain key features are still missing from the theory: in particular 'yield' in the glassy response, and the important effects of molecular weight distribution. Secondly, the computational complexity involved in implementing a large deformation model with all the features of the molecular theory would be prohibitive for present-day computing resources, for realistic simulations of stretching flow processes.

In this situation, we adopt the approach employed in previous work on hot-drawing of poly(ethylene terephthalate) (PET), and take as a starting point the 'glass–rubber' constitutive model proposed by Buckley and Jones [3], modified to include relaxation of σ^c as proposed by Adams et al. [4], but without the additional feature of stress crystallisation needed in the case of PET. This model is three-dimensional, encompasses large deformations, and captures the major features of response observed experimentally on either side of the glass transition. It is *quasi*-physical: in particular limiting cases, it agrees with molecular theory, but in general, it differs in its detailed predictions. An important practical question is whether any of these differences are significant. The key advantage of the model is that it appears to be a useful engineering compromise. It captures polymer behaviour to reasonable accuracy on either side of the glass transition, but also has acceptable computational efficiency, for FE models of stretching flow processes near the glass transition, as reported elsewhere for PET [5].

This paper has three aims. Firstly, we demonstrate wider applicability of the form of model proposed, by applying it to cast, high molecular weight PMMA. This material was chosen for its practical importance in the context of thermoforming, and its theoretical advantage of availability in accurately isotropic form. Moreover, with its high molecular weight and lack of any crystallisation, this material provides the ideal contrast to the low molecular weight, stress-crystallising PET polymer, where the model was applied previously. Secondly, we show how the model is extended to include a relaxation spectrum for σ^c, allowing for large elastic and viscous deformations, as needed to fit high molecular weight PMMA in detail. Thirdly, we report results from a new experimental study of the constitutive response of PMMA above T_g, in which temperature, strain-rate and strain-state are varied, and we apply the new model to the data.

2. Background

There is broad agreement among previous authors on the outline form of any constitutive model for describing deformation of amorphous polymers near the glass transition. It must combine a stress exhibiting elastic–viscoplastic response, acting in parallel with a stress that shows pronounced strain-stiffening. The present model has this form, as have previous models, from the original one-dimensional model of Haward and Thackray [6] to the fully three-dimensional model of Boyce and co-workers [7]. Indeed Haward has shown that the same form of model can even be fitted to data for semi-crystalline polymers [8].

The strain-stiffening is generally attributed to rubber-like entropic elasticity, due to the reducing entropy of aligning mobile chains, even when observed below the glass transition. Certainly, the qualitative appearance of the phenomenon below T_g is similar to that observed in the rubbery state, where there is well-established evidence for entropy domination of the free-energy change. However, it should be noted that the use of the same description below T_g has not yet been justified rigorously. In the present model, however, we follow usual practice and invoke a conformational entropy function when calculating this part of the stress. The entropy function used is that derived by Edwards and Vilgis [9], for a network of crosslinked and entangled chains where the tube constraint is represented by a series of slip links along the molecule, in the limit where the density of crosslinks is negligible. Thus, in its rubber-elastic response—obtaining on timescales $\tau_e \ll t \ll \tau_R$—the model is consistent with molecular theory. The Edwards–Vilgis model has also been applied successfully (in its earlier form ignoring finite chain extensibility [10]) to hot-stretching of PET by Matthews et al. [11] and to PVC by Sweeney and Ward [12]. Other authors have used semi-empirical descriptions of the rubber-elastic response. Kuhn's well-known 'inverse-Langevin' expression for the force acting between two junction points of a crosslinked non-Gaussian network of chains of finite length has been used. The isotropic distribution of initial end-to-end vectors was represented by a 3-chain approximation [7] or an 8-chain approximation [13], while Wu and van der Giessen claimed an empirical mix of 3-chain and 8-chain mimics best the isotropic distribution [14]. In fact it appears that, for practical purposes in fitting data, the molecularly based Edwards–Vilgis approach or the semi-empirical approaches may be equally successful.

On the other hand, there is more serious disagreement among previous authors on how relaxation of σ^c should be described. In the present model [4,5,15] and in more recent work on PET by Boyce and co-workers [16], the total deformation is decomposed into a portion that is an entropy elastic stretch (corresponding to molecular alignment due to constraint by the stretched tube) and a portion that is a viscoplastic stretch (corresponding to retraction and/or escape from the tube). A one-dimensional analogue would therefore be a spring in series with a dashpot. One such element was found to be sufficient to fit data in the case of PET [4], but as will be shown later, more than one element may be necessary. In the linear viscoelastic limit

the model is therefore consistent with the various forms of Maxwell model often used in modelling flow of elasto-viscous fluids: in this limit it is also consistent with the molecular theory. The latter results, for example, in a stress relaxation modulus in shear that is a sum of functions decaying exponentially with time [1] (a Prony series), characteristic of a generalised Maxwell model.

Other authors, however, have taken a different approach. The inability of a purely hyperelastic network model to describe orientation or constitutive response in thermoplastics at large strains has been interpreted as evidence for an entropy-elastic network with variable chain density: reducing with increasing time, temperature or strain during deformation. Several authors deduce the network chain density to be temperature-dependent. Examples are Raha and Bowden [17], Arruda et al. [18], and G'Sell and Souahi [19] all of whom applied this approach to PMMA. These authors assume the density of entanglement junction points in the network to decay with increasing temperature according to a thermally activated process (although Raha and Bowden refer to 'cohesion points' rather than entanglements).

Within a deformation experiment at fixed temperature, the inability of a network to account quantitatively for birefringence changes in PMMA has been attributed to the network chain density decaying with increasing *strain*, as also proposed by Raha and Bowden [17]. These authors found that an exponential decay fitted their data. Later work by Botto et al. [20] showed that, although Raha and Bowden's approach could fit birefringence data during drawing of PMMA just below the glass transition at 90 °C, it provided a very poor fit above T_g at 135 °C, and also noted that the theory produced the unphysical result of zero birefringence at large strains. They therefore modified the model to include two networks acting in parallel, a permanent network with N_p chains per unit volume, and a temporary network of N_t chains per unit volume in the unstrained state which breaks down on deformation. Using this approach, they obtained a good fit to data both below and above the glass transition. It is significant for the present work that two networks were necessary. One might regard the N_p network as the *fraction* of the network with a substantially higher viscosity than the relaxing N_t network. Sweeney and Ward [21] later re-examined the approach of Botto et al. using the slip-link model of Ball et al. and extended the representation to three dimensions, by allowing the slip-link density N_s to be a function of the first stretch invariant I_1. To accommodate the fact that a constant network also cannot describe the variation of drawing stress with strain-rate, Sweeney and Ward, working on PVC [12], and Matthews et al. working on PET [11], modelled biaxial drawing by allowing N_s to increase linearly with the logarithm of the octahedral shear strain-rate.

It is clear from such work that satisfactory empirical fits to data can be achieved by a network model with varying chain density. This approach is also computationally efficient when employed in a numerical model. There are, however, two major difficulties. Firstly, there is the theoretical objection of a lack of contact with the molecular theory, and correspondingly a lack of convergence on the known generalised Maxwell-model type of response in the linear viscoelastic limit. Secondly, there is the practical objection that each empirical description in terms of a variable network chain density applies only to a particular context: for example monotonically increasing strain, and constant strain-rate and temperature. Any non-trivial FE simulation of polymer response in a product or process, however, will involve situations of unloading, and varying strain-rate and possibly temperature. Under these conditions such a model is insufficiently defined, and predicts unphysical response.

Such deficiencies are not shared by the glass–rubber constitutive model employed in the present work. However, potentially, it does pose a different problem: the significant computational effort involved in modelling the network and multiple viscous relaxation processes at large deformations. This difficulty could render the approach impractical, despite its theoretical advantages. The principal aim of this paper, therefore, is to investigate the practicality of introducing a spectrum of network relaxations to model PMMA. We demonstrate that it is possible to represent the behaviour with the small number of relaxation processes required for numerically efficient FE analyses, and we show how the parameter set may be obtained.

There is little published data with which to assess the performance of the glass–rubber model for PMMA above the glass transition (ca. 110 °C), in the time–temperature window of practical relevance to processing. The large deformation constitutive response of PMMA has been studied previously in compression at temperatures below T_g, notably by Bauwens-Crowet up to 100 °C [22] and more recently by Arruda et al. [18]. In tension, the problem of obtaining similar information is rendered more difficult, by brittle fracture intervening at temperatures below approximately 40 °C, and by necking at higher temperatures. Nevertheless, by careful measurement of strain and true stress within the neck, Hope et al. succeeded in measuring meaningful true-stress/strain relations in tension at 90 °C for a wide range of strain-rates [23]. Using a similar approach, with specially developed automated equipment, G'Sell and Souahi obtained true-stress/strain data in tension, through the glass transition from 95 to 140 °C [19]. From these earlier authors, there is also some information on the effects on the constitutive response of varying molecular weight [19,23,24], free monomer [24], and crosslinking [19]. Since, however, the work of G'Sell and Souahi did not include the important effects of varying strain-rate and strain-state, their results are insufficient to provide an adequate test for the fully three-dimensional constitutive model proposed here. Consequently, we have carried out a wider experimental study of one grade of PMMA in the temperature region of interest. In a later section, results

are interpreted in terms of the model and a set of model parameters determined.

3. The glass–rubber constitutive model

The constitutive model employed in this work is an extension of that outlined previously [4], based on a study of hot-drawing of amorphous PET under biaxial stress [4,15]. Further details of its implementation were given by Gerlach et al. [5]. The following is an outline of the existing model as applied to a non-crystallising polymer, and its generalisation as needed to model PMMA from the glass transition to thermoforming temperatures.

3.1. Existing model

For applicability within the FE context, the purpose of the model is to compute the Cauchy stress tensor at time t, for a given history of the three-dimensional deformation field $\mathbf{x}(\mathbf{X})$, where $\mathbf{x}$ and $\mathbf{X}$ are the current and initial positions, respectively, of any material particle. The physical basis of the model is the knowledge that there are two dominant sources of strain-induced free energy change in a polymer—perturbation of inter-atom potential energy (giving the 'bond-stretching' stress σ^{b}), and perturbation of chain conformational entropy (giving the 'conformational' stress σ^{c}). The key assumption of the model is that these act independently, subject to the same deformation, as expressed through the deformation gradient tensor $\mathbf{F}$. Thus there is parallel coupling between them, which may be expressed in terms of $\mathbf{F}$ and the Cauchy stress tensor $\boldsymbol{\sigma}$ as follows

$$\mathbf{F} \equiv \frac{\partial \mathbf{x}}{\partial \mathbf{X}} = \mathbf{F}^{b} = \mathbf{F}^{c}, \tag{1}$$

$$\boldsymbol{\sigma} = \boldsymbol{\sigma}^{b} + \boldsymbol{\sigma}^{c}. \tag{2}$$

Since the stress response is dominated by $\boldsymbol{\sigma}^{b}$ below the glass transition and by $\boldsymbol{\sigma}^{c}$ above it, it follows that if these are constitutively prescribed in terms of $\mathbf{F}$, the model is equally applicable above and below the glass transition. For this reason we refer to the model as a *glass–rubber constitutive model* of a polymer. In describing flow of the model below, it will be convenient to focus on the tensors of *rate* of deformation (symmetric part of the velocity gradient) giving rise to $\boldsymbol{\sigma}^{b}$ and $\boldsymbol{\sigma}^{c}$. In terms of these, Eq. (1) gives

$$\mathbf{D} = \mathbf{D}^{b} = \mathbf{D}^{c}. \tag{3}$$

In the glassy state where $\boldsymbol{\sigma}^{b}$ is dominant, perfect elasticity is not observed: elastic distortion of inter- and intra-molecular potentials cannot account for the entire deformation. There is also a viscoplastic contribution, arising from the thermally activated short-range diffusion of molecular segments. It follows that the rate of deformation $\mathbf{D}^{b}$ giving rise to $\boldsymbol{\sigma}^{b}$ is the addition of elastic and viscoplastic contributions:

$$\mathbf{D}^{b} = \mathbf{D}^{e} + \mathbf{D}^{v}. \tag{4}$$

In a similar manner, under conditions where $\boldsymbol{\sigma}^{c}$ is dominant, there is much evidence to suggest that elastic stretch of a network of constant properties cannot account for the entire deformation, as we saw in Section 2. Consequently, the corresponding rate of deformation is also decomposed into a part associated with network stretch (n) and another part associated with relaxation of molecular orientation by retraction within the tube and escape from the tube—or expressed in terms of the entanglements that define the tube, by slippage of the entanglements (s):

$$\mathbf{D}^{c} = \mathbf{D}^{n} + \mathbf{D}^{s}. \tag{5}$$

Eqs. (3)–(5) are the key *kinematic* assumptions of the model. They differ in detail from those employed in the similar model proposed by Boyce et al. for PET [16], in that these authors invoke the alternative description, in terms of a multiplicative decomposition of the deformation gradient. For general deformations including rotations, the two approaches are not equivalent in the presence of large elastic stretches, as encountered in the present work in the network response.

The hydrostatic part of the bond-stretching response is taken to be linear elastic with bulk modulus K^{b}. The mean stress σ_{m}^{b} and the volume ratio J are defined by

$$\boldsymbol{\sigma}_{m}^{b} \equiv \tfrac{1}{3} tr(\boldsymbol{\sigma}^{b}); \qquad J \equiv \det \mathbf{F} \tag{6}$$

and they are related by the equation

$$\sigma_{m}^{b} = K^{b} \ln J + \sigma_{m0}^{b}, \tag{7}$$

where σ_{m0}^{b} is the initial, built-in, bond-stretching stress resisting collapse of the entropic network.

Elastic and viscous parts of the deviatoric rate of deformation, $\mathbf{D}^{e'}$ and $\mathbf{D}^{v'}$, respectively, are assumed to be governed by isotropic linear elasticity and an isotropic flow rule as follows, where $\mathbf{S}^{b}$ is the deviatoric part of $\boldsymbol{\sigma}^{b}$ and a hat denotes the time derivative with respect to a reference frame rotating with the material:

$$\mathbf{D}^{e'} = \frac{\hat{\mathbf{S}}^{b}}{2G^{b}}; \qquad \mathbf{D}^{v'} = \frac{\mathbf{S}^{b}}{2G^{b}\tau}. \tag{8}$$

Here, G^{b} is the bond-stretching contribution to the shear modulus, and the relaxation time τ is given in terms of the linear viscoelastic relaxation time τ_0 and a stress-dependent factor a derived from a three-dimensional generalisation of the Eyring flow model. Eq. (4), applied to the deviatoric part of the rate of deformation $\mathbf{D}'$, then yields the differential equation

$$\hat{\mathbf{S}}^{b} = 2G^{b}\mathbf{D}' - \frac{\mathbf{S}^{b}}{\tau}, \tag{9}$$

where $\hat{\mathbf{S}}^{b}$ (identified with the Jaumann rate of stress) and τ

are given by

$$\hat{\mathbf{S}}^{\mathrm{b}} = \dot{\mathbf{S}}^{\mathrm{b}} + \mathbf{S}^{\mathrm{b}}\mathbf{W} - \mathbf{W}\mathbf{S}^{\mathrm{b}}, \tag{10a}$$

$$\tau = a\tau_0; \qquad a = \frac{\exp\left(\dfrac{-V_{\mathrm{p}}\Delta\sigma_{\mathrm{m}}^{\mathrm{b}}}{RT}\right)}{\sinh\left(\dfrac{V_{\mathrm{s}}\tau_{\mathrm{oct}}^{\mathrm{b}}}{2RT}\right)}\frac{V_{\mathrm{s}}\tau_{\mathrm{oct}}^{\mathrm{b}}}{2RT}. \tag{10b}$$

In Eqs. (10a) and (10b), $\mathbf{W}$ is the spin tensor, $\tau_{\mathrm{oct}}^{\mathrm{b}}$ is the octahedral shear stress and $\Delta\sigma_{\mathrm{m}}^{\mathrm{b}}$ is the strain-induced mean stress $\sigma_{\mathrm{m}}^{\mathrm{b}} - \sigma_{\mathrm{m0}}^{\mathrm{b}}$, while V_{s} and V_{p} are the shear and pressure activation volumes, respectively. Details of the derivation of a are given elsewhere [3].

Dependence of the viscoelastic relaxation time on temperature T and structure (via fictive temperature T_{f}) is expressed through the equation:

$$\tau_0 = \tau_0^* \exp\left(\frac{C}{T_{\mathrm{f}} - T_\infty} - \frac{C}{T_{\mathrm{f}}^* - T_\infty} + \frac{\Delta H_0}{RT} - \frac{\Delta H_0}{RT^*}\right), \tag{11}$$

where τ_0^* is the linear viscoelastic relaxation time for a reference temperature T^* and structural state (fictive temperature) T_{f}^*. Again, the reader should refer to Buckley and Jones [3] for the detailed derivation. Above the glass transition, where structural equilibrium obtains $T_{\mathrm{f}} = T$, and Eq. (11) reduces to that employed by Macedo and Litovitz [25].

Consider now the conformational contribution to the stress. Entropic elasticity of the entanglement network is expected to be highly non-linear, because of the finite extensibility of chains. This explains strain-stiffening in amorphous polymers above the glass transition, and is usually assumed to explain it below T_{g} in addition. It is convenient therefore to calculate the conformational stress directly by differentiation of the conformational free energy density A^{c}. Theories of rubber elasticity yield expressions for A^{c} in terms of the principal network stretches λ_i^{n} ($i = 1\ldots3$). Thus, the principal components of the Cauchy stress are obtained from

$$\sigma_i^{\mathrm{c}} = \frac{1}{J}\frac{\partial A^{\mathrm{c}}(\lambda_1^{\mathrm{n}}, \lambda_2^{\mathrm{n}}, \lambda_3^{\mathrm{n}})}{\partial \ln\lambda_i^{\mathrm{n}}}. \tag{12}$$

In the present work, the Edwards and Vilgis [9] expression for A^{c} has been employed. It was derived for the case of a network of freely orienting chains of finite length, where the tube constraint is approximated by junction points of a physical nature with some freedom of movement (i.e. entanglements)—the slip-links. The network behaviour of uncrosslinked PMMA can be modelled as a form of Edwards–Vilgis rubber, in the limit where there are no chemical crosslinks:

$$A^{\mathrm{c}}(\lambda_1, \lambda_2, \lambda_3) = \frac{N_{\mathrm{s}}k_{\mathrm{B}}T}{2}\left[\frac{(1+\eta)(1-\alpha^2)}{1-\alpha^2\sum_{i=1}^{3}\lambda_i^2}\sum_{i=1}^{3}\frac{\lambda_i^2}{1+\eta\lambda_i^2} + \sum_{i=1}^{3}\ln(1+\eta\lambda_i^2) + \ln(1-\alpha^2\sum_{i=1}^{3}\lambda_i^2)\right], \tag{13}$$

where N_{s} is the number density of slip-links, η is a parameter specifying the looseness of the entanglements ($\eta = 0$ for a crosslink), and α is a measure of the inextensibility of the entanglement network. It is related to the number n of freely orienting (Kuhn) segments per network chain: $\alpha = \sqrt{n^{-1}}$). The Edwards–Vilgis model is a further development of the model of Ball et al. [10], and in the limit that the inextensibility α is vanishing small, implying a large number of Kuhn segments per chain, is equivalent to the Ball model.

Completion of the model requires a representation of the relaxation of conformational stress by molecular diffusion along the tube: in the language of entanglements—entanglement slip. Such an extension of the original model was discussed in detail by Adams et al. for PET [4], with further details on its implementation given by Gerlach et al. [5]. For PMMA, extension of the Buckley–Jones model [3] to include entanglement slippage is in principal more straightforward, as there is no crystallisation process to modify the rate of flow. To minimise complexity, an isotropic, isochoric Newtonian flow rule is invoked and the slippage rate of deformation appearing in Eq. (5) is then given by:

$$\mathbf{D}^{\mathrm{s}} = \frac{\mathbf{S}^{\mathrm{c}}}{\gamma}, \tag{14}$$

where γ is a slippage viscosity that depends only on temperature. The failure to capture non-Newtonian flow will render the model inaccurate at high rates of deformation, but this form was sufficient at the rates employed in the present tests (see below). It may be noted that, although the slippage *viscosity* is assumed constant, because the network strains are large the conformational behaviour is non-linear viscoelastic. The equivalent relaxation time depends on the stretch-dependent hyperelastic moduli, and so is neither constant nor isotropic. Consequently, it is not helpful to work in terms of a slippage relaxation time (or times), and throughout the model we define slippage behaviour in terms of viscosities. The temperature dependence of the slippage

viscosity is modelled in terms of the Fulcher equation

$$\gamma = \gamma^* \exp\left(\frac{C^s}{T_f - T_\infty^s} - \frac{C^s}{T_f^* - T_\infty^s} \right), \quad (15)$$

where again we have $T_f = T$ above the glass transition, and the limiting or Vogel temperature T_∞^s for the slippage process may not in general be identical to that for the segmental flow process.

3.2. Extension of the constitutive model

In a previous paper [26], two of us outlined the extension of the glass–rubber constitutive model to a model with a spectrum of bond-stretching relaxation times, and found success in accounting for key features of the non-linear viscoelastic response in the glassy state of PMMA. There was assumed to be a single elastic shear modulus G^b, but a range of N activation energies and entropies, giving rise to a distribution of N relaxation times. Polymer with the jth relaxation time was taken to account for a volume fraction v_j of the total volume of the glass, replacing Eq. (2) by

$$\boldsymbol{\sigma} = \sum_{j=1}^{N} v_j \boldsymbol{\sigma}_j^b + \boldsymbol{\sigma}^c \qquad \text{with} \sum_{j=1}^{N} v_j = 1. \quad (16)$$

To provide detailed modelling of flow *above* the glass transition, we now extend the model to include an arbitrary number P of different network relaxations, so that the total Cauchy stress tensor becomes:

$$\boldsymbol{\sigma} = \sum_{j=1}^{N} v_j \boldsymbol{\sigma}_j^b + \sum_{k=1}^{P} w_k \boldsymbol{\sigma}_k^c \qquad \text{with} \sum_{j=1}^{N} v_j = \sum_{k=1}^{P} w_k = 1. \quad (17)$$

In fact, in the present application—modelling of large deformations of PMMA above the glass transition—the bond-stretch stress makes only a small contribution and it is sufficient to take $N = 1$; but we show later that the data require $P > 1$. This is consistent with the tube model of relaxation of the conformational stress, that results in a relaxation spectrum. In addition, in a polydisperse polymer there is likely to be a further contribution to the spectrum arising from heterogeneity of the entanglement network, since relaxation times are predicted by the tube model to have strong dependence on molecular weight (M). For example, $\tau_R \sim M^2$ and $\tau_d \sim M^3$ (see Doi and Edwards [1]). If heterogeneity is the dominant cause of the spectrum, the weighting factor w_k in Eq. (17) is the number fraction of slip-links associated with a viscosity γ_k. Whatever the cause, Eqs. (5) and (14) are replaced by the sets of equations

$$\mathbf{D}^c = \mathbf{D}_k^n + \mathbf{D}_k^s \text{ where } \mathbf{D}_k^s = \frac{\mathbf{S}_k^c}{\gamma_k} \qquad (k = 1...P). \quad (18)$$

It follows that, at any instant, there is a range of slippage rates of deformation, and hence a range of rates of network deformation, which with appropriate integration yield the corresponding principal network stretches λ_{ik}^n ($i = 1...3$, $k = 1...P$). Each principal conformational stress is then obtained by generalising Eq. (12)

$$\sigma_{ik}^c = \frac{1}{J} \frac{\partial A^c(\lambda_{1k}^n, \lambda_{2k}^n, \lambda_{3k}^n)}{\partial \ln \lambda_{ik}^n} \qquad (i = 1...3,\ k = 1...P). \quad (19)$$

In evaluating Eq. (19), we assume the nature of the slip-links and the length of network chains between entanglements to be common to the whole material, since they depend only on the chemical structure of the monomer and are independent of M. Hence common values of N_s, α and η are employed. It is clear from Eqs. (17) and (18) that the resulting model, in the linear viscoelastic limit is a generalised Maxwell model in shear. This agrees with the molecular theory. If G_N^0 is the rubbery plateau shear modulus, the linear viscoelastic relaxation time corresponding to γ_k is $\tau_k = \gamma_k/2G_N^0$. By assigning the values $w_k = 8/\pi^2 k^2$ and $\tau_k = \tau_d/k^2$ for k odd, and zero otherwise, with P very large, we can if we wish retrieve the Doi–Edwards spectrum [1] for a monodisperse linear polymer in the linear viscoelastic limit. For practical engineering purposes, however, there is every incentive to keep P as small as possible and to fit w_k and γ_k empirically.

In the present work, the entire constitutive model was implemented numerically in FORTRAN, as a fully three-dimensional user material subroutine (UMAT) suitable for use with the commercial large-strain FE code ABAQUS. The predicted responses of the model reported below were computed using a 'stepper' program that simulated ABAQUS in its interactions with the subroutine. For a given history of $\mathbf{F}$ and temperature, the stress tensor was calculated as a function of time, by numerical integration of the equations of the model. In the design of the UMAT, considerable attention was paid to achieving numerical accuracy, stability and efficiency, and it has performed satisfactorily within ABAQUS in modelling of large inhomogeneous deformations of cast PMMA in sheet form. Further details lie beyond the scope of the present paper.

4. Experiments

4.1. Material

The polymer used in this work was ICI PMMA homopolymer in the form of cast sheet supplied by ICI Acrylics (now Ineos Acrylics). This is the conventional high molecular weight form of PMMA with weight average molecular weight approximately 10^6 Da. One grade (PMMA1) of nominally 1 mm thick sheet was used for all the tensile experiments described in this paper, and a second grade (PMMA2) of nominally 2 mm thick sheet was used for all the compressive tests. A small difference of less than 5 K in the glass transition temperatures of the two grades was apparent both from the mechanical tests and from DSC studies. This is believed to be due to the presence of a very

small proportion of low molecular weight polymer or oligomer in PMMA2. There was no chemical cross-linking present in either grade.

4.2. Specimens

Before machining, the cast PMMA was normalised to remove even the slightest residual anisotropy from the casting process, and to ensure that the specimens all had the same initial thermal history, and were free of any residual thermal stress. The normalisation process involved: heating from ambient to 140 °C at 1 °C per minute; holding at a constant temperature of 140 °C for 20 min; slow cooling at 4 °C per hour down to 103 °C; maintaining this temperature for 20 min and then slow cooling at 4 °C per hour down to ambient temperature. From the cast and normalised sheets, specimens were prepared for uniaxial tension and compression tests, by means of numerically controlled machining, with each specimen cut individually and without coolant. Tensile specimens were of dumbbell geometry with a width of 5 mm and straight-sided gauge length of length 80 mm. The compression specimens consisted of circular disks of diameter 10 mm, cut individually from the second batch of 2 mm thick sheet and stacked five at a time to form a cylinder with a ratio of diameter: height of approximately 1:1.

4.3. Test procedures

All tests were carried out isothermally, using an Instron 4204 testing machine and an Instron 3119 Series Temperature Controlled Chamber (Model EC30), with 3119–004 high-temperature pneumatic grips used in the tensile tests. The Instron Series IX Automated Materials Tester Version 7.51 software package was used to control the tests and acquire data. All of the experiments in this study were conducted at constant cross-head speed, i.e. at constant rate of nominal strain. The raw load-displacement data were then processed into stress–strain data using in-house software. For both tensile and compression tests, true stress was calculated from the nominal stress and axial nominal strain, assuming incompressibility.

To ensure reproducible thermal histories and freedom from residual machining stresses, all specimens were given a further heat-soak at the test temperature or at 140 °C (whichever was the higher) for 20 min, before taking them to the test temperature for the start of testing. A 5 kN load cell was used for all the compressive tests and the lower temperature tensile tests, with a 100 N load cell used for the high temperature tensile tests. The load cells were air-cooled with a fan (without this precaution calibration was often impossible above 150 °C). Maximum nominal strain-rates were 0.75 (tension) and 3.5 min^{-1} (compression); higher values being avoided, to minimise adiabatic heating.

4.4. Tensile tests

The thermal inertia of the pull-rod connected to the upper pneumatic grip caused delays in achieving uniformity of specimen temperature. The temperature of the upper grip was therefore monitored continually with a thermocouple, to ensure a uniform specimen temperature prior to testing. The general procedure for tensile tests below 140 °C was as follows.

(i) The specimen was placed in the oven and gripped in the upper pneumatic grip, with a fine thermocouple junction located adjacent to the specimen. The lower grip was left open to allow for thermal expansion.
(ii) The oven temperature was raised to 140 °C and maintained at this temperature for at least 20 min.
(iii) The oven was cooled down to the test temperature and maintained at this temperature for a period of 10 min to ensure stability.
(iv) The oven fan speed was reduced to its lowest setting to avoid disturbance to the specimen, and the lower pneumatic grip was closed.

For tests at temperatures above 140 °C a similar procedure was followed, except that the heat-soak was at the test temperature and there was no cooling down phase.

To check the uniformity of the deformation tests, the specimens were marked with a series of horizontal lines 8 mm apart over the gauge length region of the specimen. The strain in the marked region at the end of the test was calculated and compared with the strain given by dividing the final Instron displacement by the specimen gauge length for a representative sample of tests over a range of strain rate from 0.8 per minute down to 0.05 per minute and final strains ranging from 0.66 to 2. It was found that the displacement as measured by the Instron overestimated the true displacement in the gauge length, but only by a small amount, caused by the specimen slipping slightly in the pneumatic grips. The average error in the strain obtained from the Instron data compared with the strain measured from the displacement of the marked lines was 2.43%, and the median error was 2.13%, comparable with uncertainty in the data from other sources. Therefore, displacement values recorded by the testing machine were used without correction in computing tensile strain in the guage length. No discernible necking was apparent in the present series of tests.

4.5. Compression tests

In order to capture fully the strain-state dependence of yield and flow, it was necessary to carry out tests under two different strain states (recall that the stress dependence of the viscoelastic relaxation time depends on *two* material parameters: V_s and V_p). This objective was met by combining results from uniaxial compression tests with those from tension tests. Compression tests were carried out using

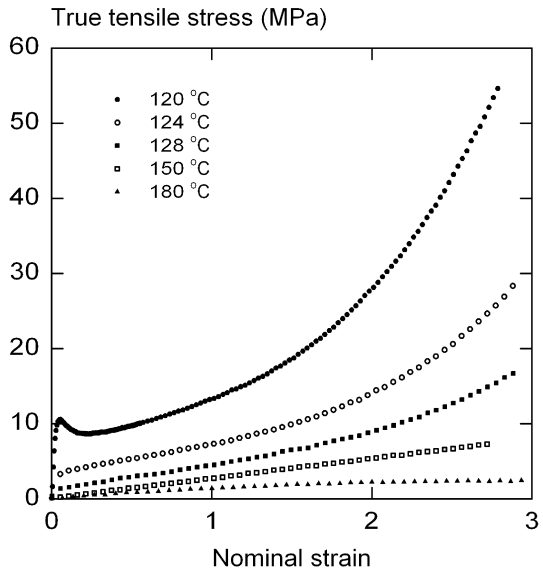

Fig. 1. Example plots of true stress versus nominal strain data for uniaxial drawing of sample PMMA1 at a nominal strain rate of 0.4 min^{-1} and various temperatures as shown.

Instron compression platens, with the same oven as used for tension, and following the same thermal sequence prior to the start of testing. The disk specimens were stacked and aligned on the lower platen using a specially designed PTFE tool. To check that the specimens were deforming uniaxially in the strain range of interest around yield, the compression tests were recorded on video tape.

Barrelling was minimised by placing a layer of PTFE film between the specimen and the platens. In the range of negative true strain and strain rates of interest in the present work, barrelling was not significant, as demonstrated by the reproducibility of the stress–strain curves.

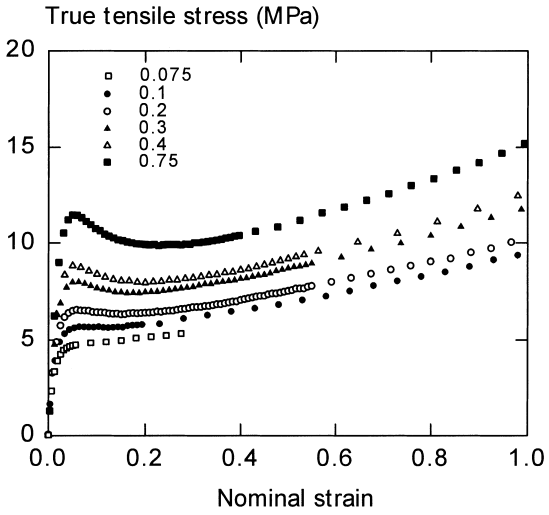

Fig. 2. Example plots of true stress versus nominal strain data for uniaxial drawing of sample PMMA1 at a temperature of 120 °C and various nominal strain rates as shown.

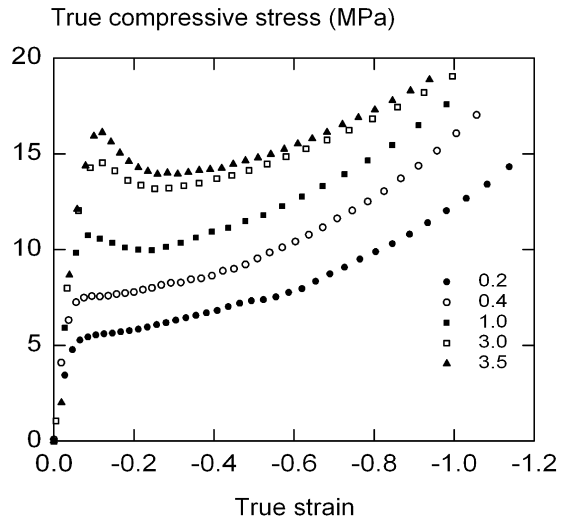

Fig. 3. Example plots of true stress versus true strain data for uniaxial compression of sample PMMA2 at a temperature of 115 °C and various nominal strain rates as shown.

4.6. Results

Fig. 1 shows examples of stress–strain data obtained in tension at a range of temperatures from 120 to 180 °C at a nominal strain rate of 0.4 min^{-1}. At the lowest temperature the stress–strain curve shows a pronounced yield peak followed by true stress-softening, then flow where stress changes only slowly, followed by significant strain-stiffening. As the temperature is increased the level of stress in the initial 'yield' region drops rapidly, reflecting the pronounced temperature sensitivity of the relaxation time τ_0 above the glass transition (where $T_f = T$ in Eq. (11)). The other major feature of Fig. 1 is the sharp decline in strain-stiffening as the temperature rises. In terms of the present model, this reflects the absence of chemical cross-links in the PMMA network. The rapid fall in the viscosities γ_k with increasing temperature, predicted by Eq. (15), causes the entanglement slippage contribution λ^s to the total stretch λ to increase, and correspondingly the network contribution λ^n and the resulting conformational stress to decrease.

Figs. 2 and 3 shows examples of stress–strain data obtained in uniaxial tension and compression, for a range of nominal strain-rates. At the highest strain-rates there is considerable true stress softening following yield in both tension and compression. Its presence in the compression data confirms that it is a genuine feature of the material and not an artefact due to undetected necking. Similar effects were observed in tension tests on PMMA at 90 °C by Hope et al. [23,24].

5. Fitting the constitutive model to data

For a constitutive model of the complexity of that

proposed here, a major question in applying it is how the numerous parameters may be found from a given data set, with confidence that they represent the best fit to the data. In the present work, the model was tested against the experimental data and best values of the parameters found, by using an extension of the systematic approach described before for PET [4]. It was done in two stages. First, where key features of the material response could be isolated unambiguously from experimental data, this was done and they were least-squares fitted separately to the corresponding equations in the model. This approach was applied to the glass-like yield response. Second, for the remaining rubber-like response (entanglement network and slippage), the whole model was used in conjunction with a commercial optimisation software package (NAG routine E04FDF). By optimising the fit of experimental data to simulations of tensile drawing experiments at various temperatures, the remaining parameters were found. Details are given later.

5.1. T_g variation

The experimental work to fit the model parameters was carried out using the two grades of PMMA with slightly different glass transition temperatures. As the majority of the experimental work was carried out on sample PMMA1, the model parameters were found for this grade: data from sample PMMA2 were used only to determine parameters that are independent of temperature. The existence of this type of T_g variation illustrates an important practical point: model parameters will in general need to be adjusted slightly for each grade of PMMA. This does not mean, however, that all the model parameters would need to be re-fitted. All that would be required would be to 'calibrate' a grade of the cast PMMA by measuring its T_g and to shift accordingly the parameter T_∞ that fixes the polymer response on the temperature scale.

5.2. Identification of the rubbery plateau

We first test the core hypothesis of the model: that the material stress response contains two separate components—arising from bond-stretch potentials and conformational entropy—relaxing on widely differing time/temperature scales. Isometric plots of stress versus temperature were generated for a range of strain levels, following the procedure applied before to PET. A typical result can be seen in Fig. 4, where the stress has been divided by absolute temperature T (since $\sigma^c \propto T$ from Eqs. (12) and (13)). A horizontal 'rubbery' plateau between 134 and 140 °C can be seen clearly. In this region, $\mathbf{S}^b$ is fully relaxed on the time-scale of the experiment, but σ^c has not commenced relaxing significantly. This demonstrates the separability of the two components of stress assumed in the model. Above 140 °C the true stress begins to fall again, although very gradually. It should be noted that the existence of the rubbery plateau does not mean that a hyperelastic material model would accurately simulate behaviour at these temperatures. At larger strains, the longer time available in the experiment could allow relaxation of $\boldsymbol{\sigma}^c$ to intervene.

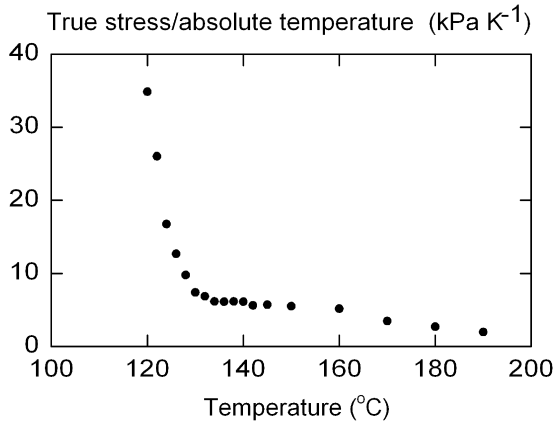

Fig. 4. Isometric plot of true tensile stress at uniaxial stretch $\lambda = 1.85$ as a function of temperature, for uniaxial drawing of sample PMMA1 at a nominal strain-rate of 0.4 min^{-1}. The stress has been normalised with respect to the absolute temperature so that a rubbery entropic response would produce a horizontal line. The rubber-like plateau is in evidence between 134 and 140 °C.

5.3. Glass-like response

The relaxation of $\mathbf{S}^b$, constituting glass-like viscoelasticity, was represented by only one relaxation time in the present work, and it was possible to fit the corresponding parameters manually, in a similar manner to that used before for PET [4]. The instantaneous elastic moduli for PMMA were taken from the previous work of two of us on the creep behaviour of the material [26]: $G^b = 0.83$ GPa and $K^b = 2.12$ GPa, with temperature-dependence neglected.

From data such as given in Figs. 1–3, it is clear that yield occurs at strains of ca 0.1 or less, and under these conditions the conformational stress makes a negligible contribution. According to the model, provided the argument of the sinh term in Eq. (10) is unity or larger, the condition for yield is given as follows in terms of the mean stress, octahedral shear stress and the shear component of $\mathbf{D}$ on the octahedral plane: σ_m, τ_{oct} and d_{oct}, respectively (see Buckley and Jones [3])

$$\frac{V_s \tau_{oct}}{2RT} + \frac{V_p \sigma_m}{RT} = \ln d_{oct} + \ln\left(\frac{\mu_0 V_s}{RT}\right). \tag{20}$$

where μ_0 is the linear limit viscosity ($\mu_0 = 2G^b\tau_0$). In the case of yield in uniaxial tension we have $\tau_{oct} = \sqrt{2}\sigma_y/3$, $\sigma_m = \sigma_y/3$, $d_{oct} = \dot{\lambda}/\sqrt{2}\lambda$ and hence Eq. (20) becomes after re-arrangement

$$\frac{\sigma_y}{T} = \frac{6R}{2V_p + \sqrt{2}V_s}\left[\ln\left(\frac{V_s\mu_0}{\sqrt{2}RT}\right) + \ln\left|\frac{\dot{\lambda}}{\lambda}\right|\right]. \tag{21}$$

Eq. (21) predicts that a plot of yield stress divided by absolute temperature versus the natural logarithm of the

true strain rate will be a straight line with gradient

$$m_t = \frac{6R}{\sqrt{2}V_s + 2V_p}. \quad (22)$$

for uniaxial tension. Similarly, for uniaxial compression where σ_m changes sign, a straight line will be obtained with gradient

$$m_c = \frac{6R}{\sqrt{2}V_s - 2V_p}. \quad (23)$$

The two lines have a common origin at

$$\left|\frac{\dot{\lambda}}{\lambda}\right| = \frac{\sqrt{2}RT}{V_s\mu_0} \quad (24)$$

and the ratio of yield stresses in tension and compression is independent of $|\dot{\lambda}/\lambda|$ and equal to

$$\frac{\sigma_{yc}}{\sigma_{yt}} = \frac{1 + \sqrt{2}V_p/V_s}{1 - \sqrt{2}V_p/V_s} \quad (25)$$

as deduced long ago by Bauwens-Crowet [22], invoking a pressure-modified von Mises yield criterion of the form represented by Eq. (20). Solving Eqs. (22) and (23) for the activation volumes we obtain

$$V_s = \frac{3R}{\sqrt{2}}\left(\frac{1}{m_t} + \frac{1}{m_c}\right); \qquad V_p = \frac{3R}{2}\left(\frac{1}{m_t} - \frac{1}{m_c}\right). \quad (26)$$

From curves such as those in Figs. 1–3, yield stresses were determined as the true stress at the peak or sharp change in gradient. Results for tension and compression are plotted in the manner described earlier in Fig. 5. Although there is noticeable scatter, attributable to the high temperature-sensitivity of the yield stress in this temperature range, the higher gradient for compression than for tension expected from Eq. (22) and (23) is clearly discernible. Least-squares fits to the two data sets gave $m_t = 7.07 \times 10^3$ and $m_c = 9.14 \times 10^3$ Pa/K, giving values for the activation volumes of 4.42×10^{-3} m^3 mol^{-1} for V_s and 0.399×10^{-3} m^3 mol^{-1} for V_p. The corresponding ratio for the yield stress ratio from Eq. (25) is 1.29—very close to the value of 1.3 that seems to be common, if not universal, in the literature among measurements on glassy polymers.

The reference viscosity μ_0^* was found from the intercept c_t of the graph for tension in Fig. 5, using:

$$\mu_0^* = \frac{\sqrt{2}RT}{V_s}\exp\left(\frac{c_t}{m_t}\right) \quad (27)$$

giving a value of 4.59 GPa s at 120 °C, which was chosen as the reference temperature T^*. The corresponding linear limit viscosity for the compression tests, using sample PMMA2, was found to be 1.31 GPa s at the lower temperature of 115 °C, suggesting a difference in T_g between the two grades of approximately 6 °C. In plotting Fig. 5, to avoid confusion, the compression data have been shifted vertically to take account of the difference in T_g.

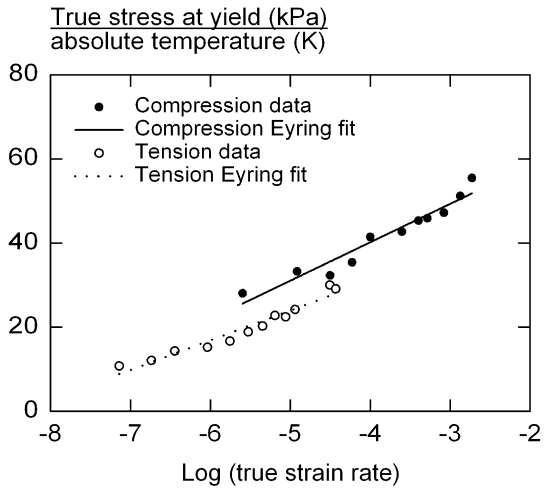

Fig. 5. Combined Eyring plot for uniaxial drawing of sample PMMA1 and compression of sample PMMA2 at 120 °C: true stress at yield divided by the absolute temperature versus the natural logarithm of the natural strain rate at yield. The points for PMMA2 have been shifted vertically to account for the difference in the glass transition temperature of the two samples.

5.4. Temperature-dependence of glassy response

The temperature-dependence of the viscosity μ_0 was found for temperatures up to 130 °C from measurements of true yield stress in tension tests at various strain rates and a range of temperatures, using the values of V_s, V_p already determined at the reference temperature. At the highest temperatures, the yield stress decayed to the extent that the condition for validity of Eq. (20) was not satisfied, and the viscosity was calculated from the tensile yield stress without approximation of the hyperbolic sine (see Adams et al. [4] for the same approach applied to constant width

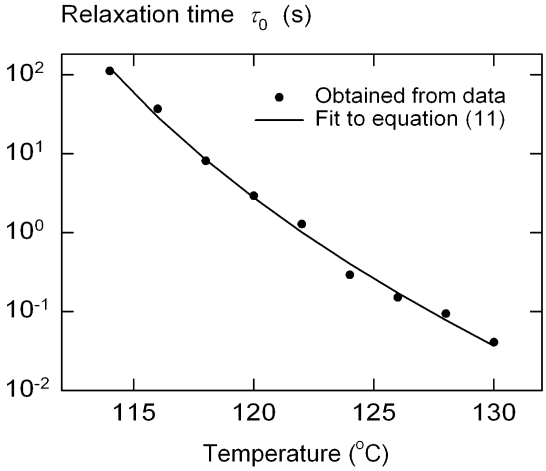

Fig. 6. Bond-stretching relaxation time $\tau_0 (= \mu_0/2G^b)$ plotted versus temperature, for sample PMMA1. The curve shown is a best fit to Eq. (11) with $T_f = T$.

drawing):

$$\mu_0 = \frac{\lambda}{\dot{\lambda}} \frac{2\sqrt{2}RT}{V_s} \exp\left(\frac{\sigma_{yt} V_p}{3RT}\right) \sinh\left(\frac{\sigma_{yt} V_s}{3\sqrt{2}RT}\right). \quad (28)$$

Eq. (11) was re-arranged to give, for temperatures above T_g where $T_f = T$

$$\ln\left(\frac{\tau_0}{\tau_0^*}\right) - \frac{\Delta H_0}{RT} + \frac{\Delta H_0}{RT^*} = \frac{C}{T - T_\infty} - \frac{C}{T^* - T_\infty} \quad (29)$$

and the activation enthalpy ΔH_0 for PMMA in the T_g region was obtained from the earlier unpublished work of Babaiikochekseraii [27] as 289 kJ/mol. The values of μ_0 were used to compute the left hand side of Eq. (29), and T_∞ was then optimised to give the best linear relation between the left hand side and $1/(T - T_\infty)$. Finally C was found from the gradient. The result was $T_\infty = 96$ °C; $C = 173.9$ K (± 0.7 K). Fig. 6 shows the temperature-dependence of the linear-limit relaxation time τ_0 together with the fitted Macedo and Litovitz equation (Eq. (11) with $T_f = T$). As can be seen, this equation provides a good fit to the relaxation time over 3.5 decades, with the values of T_∞ and C found.

5.5. Rubber-like response

The remaining model parameters, characterising the rubber-like response of the PMMA, were fitted by using least-squares optimisation, with the glassy parameters already found. The optimiser needed to be applied with care, however, because the physically based constitutive model necessarily requires numerous material parameters, and the intention was to avoid unphysical combinations of parameters, that would be unreliable outside the window of the present experiments. The approach adopted was to apply the optimisation only to the minimum number of parameters.

First the assumption was made that at 120 °C, near the glass transition, the effect of entanglement slippage is negligible. This allowed a fit of data to the network parameters independently of the slippage viscosity. Under the assumption of no chemical cross-links, the corresponding parameters are the slip-link density N_s, the inextensibility factor α, and the slip-link mobility factor η. As found previously for PET, the best value of η was found to be vanishingly small ($\sim 10^{-4}$), which implies that on the rubbery plateau the entanglements are fully constrained as if they were crosslinks. The slip-link density was found to be 3.01×10^{26} m^{-3}, with α equal to 0.15. Fig. 7 shows typical data together with the model simulation at 120 °C, assuming no slippage. It can be seen that the Edwards–Vilgis rubber model employed here, with $\eta = 0$ and the values of N_s and α fitted as above, can fit well a uniaxial drawing experiment at this temperature.

The final stage in the fitting process was to find parameters describing the temperature-dependent flow due to entanglement slippage. It was found that a *single* rubbery, or conformational, relaxation process model could not represent the data at all satisfactorily, even at a particular temperature. Fitting the temperature-dependence of slippage clearly required more than one slippage relaxation time.

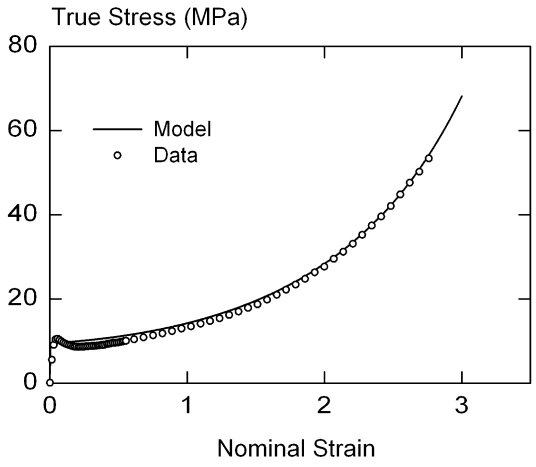

Fig. 7. True stress versus nominal strain for uniaxial drawing of sample PMMA1 at 120 °C and a nominal strain-rate of 0.4 min^{-1}: experimental data compared to the model simulation with optimised values of N_s, α and $\eta(= 0)$.

For consistency with the molecular theory, and to reduce the number of unknowns, the key assumption was made that all viscosities γ_k shared the same temperature-dependence (i.e. the same values of C^s and T_∞^s). This gave a total of $2P + 2$ parameters to find: $w_k, \gamma_k^*, C^s, T_\infty^s$. The fact that it was necessary to have more than one slippage relaxation process ($P > 1$) is demonstrated clearly in Fig. 8, which shows the difference between trying to model data for 128 °C using one or two slippage relaxations. As shown in the figure, a single relaxation time model cannot represent

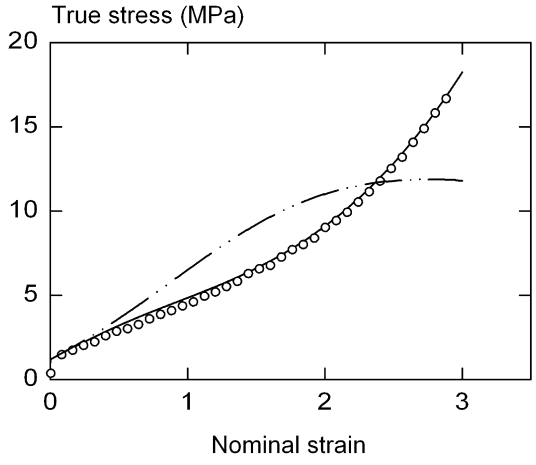

Fig. 8. Demonstration that more than one slippage viscosity is required: simulation of drawing of PMMA at a nominal strain-rate of 0.4 min^{-1} and a temperature of 128 °C using the model optimised with $P = 1$ (broken line) or with $P = 2$ (full line), compared with experiment for sample PMMA1 (data points). No reasonable fit is possible with only a single viscosity.

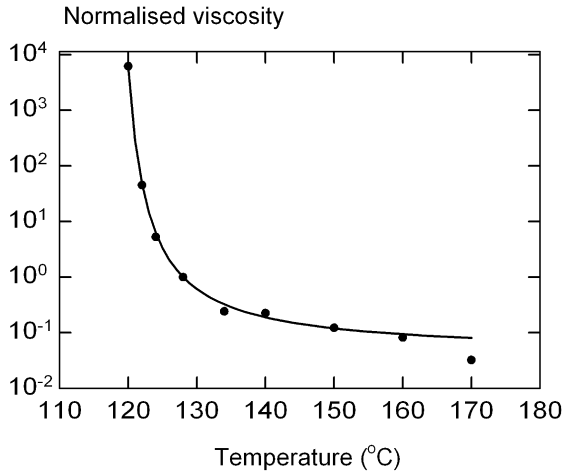

Fig. 9. Temperature-dependence of slippage viscosities normalised to their values at 128 °C (points), compared to the fitted Fulcher equation (15) with $T_f = T$.

even the shape of the stress–strain curve. On the other hand, it was found that no significant advantage was gained in fitting the present data by using more than two slippage relaxation processes. Consequently, the fit was accomplished with $P = 2$, proceeding in three stages. Firstly the optimiser was used to find w_1, γ_1^{**} and γ_2^{**} for a temperature $T^{**} = 128$ °C (recall $w_2 = 1 - w_1$). Secondly the optimiser was applied to data for other temperatures T to find the shift factor $\gamma_1(T)/\gamma_1^{**} = \gamma_2(T)/\gamma_2^{**}$, and thirdly the shift factor was least-squares fitted to Fulcher equation (15) with $T_f = T$ to obtain C^s and T_∞^s. The fit of the shift factor is shown in Fig. 9, where it can be seen that the Fulcher equation provides an excellent description of the temperature-dependence of the entanglement slippage. Finally, to confirm the internal consistency of this approach, we may note from Fig. 9 that the viscosity estimated in this way for 120 °C is of order 10^4 higher than for 128 °C. Thus the original assumption of no contribution from entanglement slippage at 120 °C was a good approximation, and no further iteration was required.

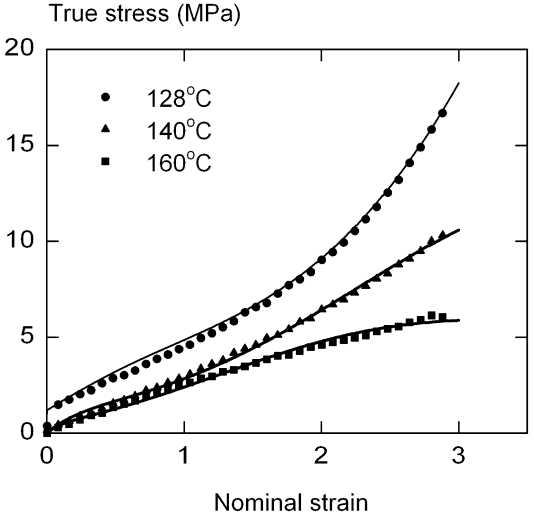

Fig. 10. Drawing of sample PMMA1 at a nominal strain-rate of 0.4 min^{-1} and various temperatures shown: comparison between experimental data (points) and the complete model with two slippage viscosities (lines), showing that the model captures the change in shape of the stress–strain curve with increasing temperature.

Table 1
Constitutive model parameters for PMMA studied in the present work. The reference temperature and structural state were: $T^* = T_f^* = 120$ °C

Parameter	Value		Source
Unrelaxed shear modulus, G	0.83 GPa		Ref. [26]
Bulk modulus, K	2.12 GPa		Ref. [26]
Glass viscosity, μ_0^*	4.59 GPa s		This work
Cohen/Turnbull constant, C	174 K		This work
Limiting temperature, T_∞	369 K		This work
Glass transition temperature, T_g	388 K		This work
Activation enthalpy, ΔH_0	289 kJ mol^{-1}		Ref. [27]
Shear activation volume, V_s	4.423×10^{-3} m^3 mol^{-1}		This work
Pressure activation volume, V_p	0.399×10^{-3} m^3 mol^{-1}		This work
Slip-link density, N_s	3.01×10^{26} m^{-3}		This work
Inextensibility factor, α	0.15		This work
Slip-link mobility factor, η	0.0		This work
Slippage Cohen/Turnbull constant, C^s	34.6 K		This work
Limiting slippage temperature, T_∞^s	390 K		This work
Slippage spectrum			
Network fractions, w_k ($k = 1, 2$)	0.677	0.323	This work
Viscosities, γ_k^* ($k = 1, 2$)	3.92 TPa s	576 TPa s	This work

Combining all these results, complete simulations were possible for the tensile drawing of PMMA across the wide temperature span from 115 to 160 °C. Fig. 10 shows the quality of the fit achieved between simulated and measured stress–strain data across this range. The complete set of parameters used in modelling the PMMA is assembled in Table 1.

5.6. Other stress states

Although the model was verified experimentally for PMMA under only uniaxial tension and compression, there is good evidence from previous work that the form of model used here would give a satisfactory representation of response under other stress states. Firstly, the multi-axial generalisation of the Eyring flow process used here implies the pressure-modified von Mises yield criterion, Eq. (20), well-known to have wide applicability to glassy polymers, and verified for amorphous PET above the glass transition [28]. Secondly, the Edwards–Vilgis free energy function has been found to capture the strain-state dependence of entropy-elastic strain-stiffening [4]. Thirdly, the entanglement slippage (network relaxation) flow process of the present model is assumed isotropic, isochoric and Newtonian: under these restrictions, its three-dimensional representation can only take the form employed here—Eq. (14).

6. Discussion

6.1. The extended model

The present work has shown that, to model the hot-drawing of even the high molecular weight polymer cast PMMA, in the temperature range of practical significance for processes such as thermoforming, it is necessary to incorporate relaxation of the rubber-elastic stress. This observation is not new. It has been noted frequently in relation to strain-stiffening below the glass transition, and also by G'Sell and Souahi in the present context of PMMA above T_g [19]. The description employed previously, however, in terms of a network with temperature-varying structure is not adequate for engineering purposes in process modelling, since the constitutive effects of temperature-*history* are not defined. The present approach overcomes this problem and provides a fully prescribed three-dimensional constitutive model. There is clearly a cost, however. We have shown that at least a modest relaxation spectrum must be invoked. Given that the elastic strains may be large in thermoforming, the extension of the original single-relaxation model [4] to include a spectrum is at some computational cost. Fortunately, for the PMMA of the present study, only a doublet relaxation spectrum was necessary.

The operation of the model, and the clear need for a multi-component representation of entanglement slippage may be seen by separating the stress into its component parts during tensile drawing: σ^b, σ_1^c and σ_2^c. In Fig. 11 a simulation is shown that reveals the contribution of each of the components to the total stress during tensile drawing at 122 °C. This temperature was chosen because at this temperature entanglement slippage has just become apparent. The glassy or bond-stretching contribution to the stress falls continuously after yield because drawing at a constant nominal strain-rate (falling true strain-rate) is being simulated. Initially both of the rubber stress curves coincide, because neither network has relaxed. At a lower temperature or a faster draw rate this would continue throughout the simulation. However, for the conditions in the simulation shown, the first fraction of the rubbery network begins to relax through entanglement slippage, while the second fraction does not relax at all during the time-scale of the simulated experiment.

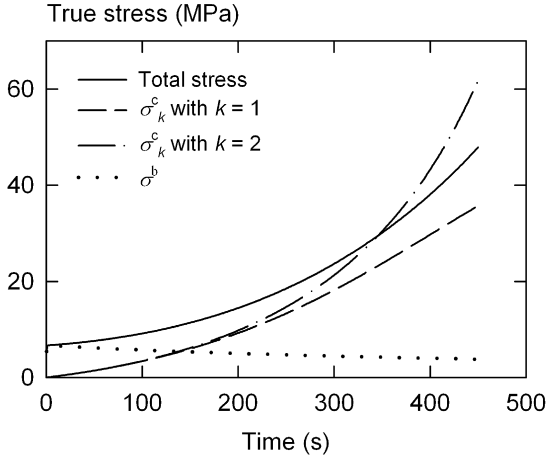

Fig. 11. Simulation of uniaxial tensile drawing of sample PMMA1 at 122 °C and a nominal strain rate of 0.4 min^{-1} (full line), showing contributions of the three different components of the model stress: conformational stresses σ_k^c with $k = 1$ and 2; and bond-stretch stress σ^b.

6.2. Glass-like response

In comparing the model simulations with experimental results in the small strain region near yield, the reader will note that the observed yield peak is not predicted by the model. This is a consequence of employing the *isostructural* assumption. We have neglected the possibility of change in the structure (de-ageing) during deformation, as would be expressed through variation in T_f. This is a deliberate simplification employed here to keep the complexity of the glass-like part of the model within bounds, since the primary interest is in the large strain response. Other recent work at Oxford [29] has shown how the restriction can be relaxed, to model better the yield of amorphous polymers below T_g. We note in this context, however, that the present results provide an interesting observation. Figs. 2 and 3 show that in the glass transition region the yield peak is a kinetic phenomenon. The yield peak is observed only at the highest strain-rates. At the slower rates the structure can presumably re-age on the time-scale of the experiment to preserve the original structure throughout.

It is instructive to compare the glass-like part of the response observed in the present work just above T_g with results of other authors obtained below T_g, since an essential feature of the model is the claimed continuity of constitutive response through the glass transition. The most comprehensive data available on the yield of PMMA below the glass transition were published many years ago by Bauwens-Crowet [22]. By employing compression tests to overcome the inherent brittleness of PMMA, she studied plastic deformation over the wide temperature range −20–100 °C. The results revealed clearly the separate contributions made by the α and β viscoelastic relaxation processes to yield in this polymer. At the high end of the temperature range, the response was shown to be dominated by the α process, as in the present work. Bauwens-Crowet also anticipated our approach by interpreting yield in terms of a three-dimensional generalisation of the Eyring theory, including the effect of hydrostatic stress. Expressing her results from compression and tension tests *at 100 °C and below* in terms of the present model, leads to values for the activation volumes of $V_s = 5.80 \times 10^{-3}$ and $V_p = 0.520 \times 10^{-3}$ kJ/mol, and hence from equation (25) a ratio of yield stresses $\sigma_{yc}/\sigma_{yt} = 1.29$. The corresponding values from the current work *above* T_g, of 4.42×10^{-3}, 0.399×10^{-3} and 1.29, respectively (see above), are satisfactorily close.

In principle, a comparison could also be made between the values deduced here for parameters C and T_∞, that govern the sensitivity of relaxation time τ_0 to the glass structure, and those obtained previously from linear viscoelastic measurements on conventional PMMA. However, the neglect by previous authors of the Arrhenius contribution to τ_0 and the scatter in reported values [30] ($C =$ 2700–5900 K and $T_\infty = 270$–320 K), vitiates any useful comparison.

6.3. The network parameters

From data obtained above the glass transition, it is interesting to compare the parameters of the entanglement network determined here with those obtained by other workers using different descriptions of the rubber-like elasticity of PMMA. If there are N_e inter-entanglement sub-chains per unit volume, this number can be related to the slip-link density through $N_e = gN_s$, where the factor g is a matter of debate in the literature. Strict interpretation of the Edwards–Vilgis model, which allows for fluctuations of network junction points, applied to a network of tetrafunctional entanglements would dictate $g = 2$. Previous authors working on the present topic, however, have invoked network models that assume affine displacement of junction points, equivalent to putting $g = 1$: this value is invoked in the following comments. The resulting sub-chain density $N_e = 3.01 \times 10^{26}$ m^{-3} may be compared with an apparent sub-chain density of close to 2.0×10^{26} m^{-3} deduced by G'Sell and Souahi [19] from data for an uncrosslinked PMMA at 120 °C, employing the Wu and Van der Giessen 3-chain/8-chain hybrid representation of non-Gaussian rubber elasticity. Similarly, 2.4×10^{26} m^{-3} was deduced for the sub-chain density by Kahar, Duckett and Ward [31] from their birefringence measurements at 116.5 °C, employing a Gaussian description. Close to the glass transition, where entanglement slippage makes least contribution, agreement is reasonable between the present work and these previous authors. The values of N_e correspond to a molecular weight M_e between entanglements in the range 2400–3612, in other words 48–72 backbone bonds. It should be noted, however, that these values lie significantly below those obtained previously from measurements of the rubbery plateau shear modulus, G^c in the model notation but normally known as G_N^0, where reported values [30] give $M_e \approx 4700$ for conventional PMMA.

The inextensibility factor $\alpha = 0.15$ obtained here suggests that there is a large number of (freely orienting) Kuhn segments between entanglements in the PMMA network: $n \approx 44$. Combining this with the values of M_e quoted earlier from hot-drawing of PMMA produces the unphysical conclusion that there are only 1.1–1.6 backbone bonds per Kuhn segment. A value of ca. 10 is implied by available values of the characteristic ratio: $C_\infty \approx 7$ (see Flory [32]). A similar inconsistency was found in the data for PET [4]. The source of the anomaly in both cases—PMMA and PET—is probably some unavoidable contribution of entanglement slippage in the apparent network response even at the lowest temperatures, close to T_g. This could lead to an underestimate of α and possibly a compensating overestimate of N_s. Another possibility is some inaccuracy in the form of the Edwards–Vilgis free energy function. On present evidence, this issue cannot be resolved.

We differ, of course, from previous authors in our intepretation of the entanglement slippage at higher temperatures. Those authors who invoke a temperature-varying network structure claim a continuous fall in chain density and increase in chain length between entanglements with increasing temperature [19]. There seems to be no other experimental evidence for such a temperature-induced change in topological structure of the melt. Indeed, given that the equilibrium topology for a linear polymer must be determined by chain flexibility and hence by chemical structure of the monomer, such a change with temperature is unlikely. The present model does not invoke such an unphysical structural change.

The other major advantage of the approach presented here is its applicability to any strain-history or temperature-history, as it is fully constitutively defined: an essential requisite for application to process modelling. The success of the extended constitutive model in simulating PMMA over such a wide temperature range suggests that the *network fraction assumption* introduced in this paper is an adequate description. The present data indicate that it is sufficient to invoke a single set of network parameters, provided different fractions of the network are allowed to relax through entanglement slippage at different rates.

As we pointed out earlier, in general it is not useful to consider the entanglement slippage behaviour in terms of relaxation times. To aid discussion, however, we can obtain the *linear-limit slippage relaxation times* at a particular temperature, using the expression

$$\tau_k = \frac{\gamma_k}{2N_s k_B T} \tag{30}$$

At a temperature of 128 °C these linear limit relaxation times are 387 and 56 836 s, respectively, and the ratio is 147. It is tempting to associate these with the two dominant relaxation times τ_R and τ_d in the tube theory, but it is clear from their ratio that this may not be justified. Theory predicts $\tau_d/\tau_R = 3.75M/M_e$ (see Doi and Edwards [1]), which exceeds 147 by an order of magnitude for the present polymer. We do not, therefore, claim that these relaxation times have any special physical significance. Rather, the two apparent relaxation processes undoubtedly represent the combined effects of a spectrum similar to that of the tube model (whose details are themselves a matter of dispute), overlaid in an ill-defined manner by effects of polydispersity and possibly some residual monomer and other non-idealities.

7. Conclusions

This paper has shown how the same glass–rubber constitutive model, that previously found success in modelling the hot drawing of PET, can (with stress-crystallisation removed) also model the hot drawing of high molecular weight PMMA. The model incorporates relaxation of the rubber-like conformational stress, enabling it to simulate the response from T_g through the thermoforming temperature range. A major advantage of the way the model is structured is that it is fully constitutively defined in three dimensions, irrespective of the loading history. This is not the case for alternative models that capture the effects of relaxation of the rubber-like network by empirical variation in the parameters of the network with strain, rate or temperature.

In the case of PMMA, however, we have shown that the representation of conformational stress relaxation requires more than the single flow process adequate for PET, and the model has been generalised to accommodate an arbitrary number of fractions of the entanglement network acting in parallel, each with a different viscosity. Although this potentially increases the number of fitting parameters without bound, in practice the problem did not arise. For PMMA, a good fit to experiment was obtained by an extension to a single network with just two fractions with different entanglement slippage viscosities. Hence, only two additional parameters were required.

Besides its practical advantages, the model benefits from having a well-defined relationship to molecular theories of polymers above the glass transition. In the limiting cases of (a) hyperelasticity on the rubber plateau, and (b) linear viscoelasticity, given the correct parameter set, it can be made quantitatively equivalent to results from the molecular theory. This is attractive for relating model parameters to molecular features.

This work has also shown that all the necessary model parameters can be obtained by performing two sets of tension tests (with varying temperature and varying strain-rate) and one set of compression tests (with varying strain-rate) on a single tension/compression testing machine. In fact, since our results have confirmed that PMMA above T_g shows the apparently almost 'universal' value of 1.3 for the ratio of yield stresses in tension and compression, tensile tests alone may be sufficient.

We believe this paper demonstrates a complete methodology for the modelling of high molecular weight PMMA in thermoforming processes above the glass transition, provided rates of deformation do not greatly exceed those employed here. It comprises a fully defined three-dimensional constitutive model that has consistency with physical theories but is structured in simpler form for greater computational efficiency in process modelling. Parameters of the model were found from constant nominal strain-rate tests in tension and compression, and systematic procedures for the data processing required to obtain these have been presented. The methods used are applicable in principle to all entangled amorphous polymers above the glass transition, close to the rubbery plateau, and we would expect the same methodology to apply to other polymers under these conditions. Thermoforming at much higher rates, however, would imply the possibility of significantly non-Newtonian flow in the entanglement slippage process, not included in the present model.

Acknowledgements

The authors are indebted to ICI plc for financial support. They are also grateful for the skilled technical assistance of Mr Neil Warland, Mr Roger Stone and Mr Ian Gloster.

References

[1] Doi M, Edwards SF. The theory of polymer dynamics. Oxford: Clarendon Press, 1986.
[2] McLeish TCB, Milner ST. Adv Polym Sci 1999;143:195.
[3] Buckley CP, Jones DC. Polymer 1995;36:3301.
[4] Adams AM, Buckley CP, Jones DP. Polymer 2000;42:771.
[5] Gerlach C, Buckley CP, Jones DP. Trans I Chem E Part A 1998;76:38.
[6] Haward RN, Thackray G. Proc R Soc 1968;A302:453.
[7] Boyce MC, Arruda EM. Polym Engng Sci 1990;30:1288.
[8] Haward RN. Macromolecules 1993;26:5860.
[9] Edwards SF, Vilgis T. Polymer 1986;27:483.
[10] Ball RC, Doi M, Edwards SF, Warner M. Polymer 1981;22:1010.
[11] Mathews RG, Duckett RA, Ward IM. Polymer 1997;38:4795.
[12] Sweeney J, Ward IM. Polymer 1995;36:299.
[13] Arruda EM, Boyce MC. J Mech Phys Solids 1993;41:389.
[14] Wu PD, Van der Giessen E. J Mech Phys Solids 1993;41:427.
[15] Buckley CP, Jones DC, Jones DP. Polymer 1996;37:2403.
[16] Boyce MC, Socrate S, Llana PG. Polymer 2000;41:2183.
[17] Raha S, Bowden PB. Polymer 1972;13:174.
[18] Arruda EM, Boyce MC, Jayachandran R. Mech Mater 1995;19:193.
[19] G'Sell C, Souahi A. J Engng Mater Technol 1997;119:223.
[20] Botto PA, Duckett RA, Ward IM. Polymer 1987;28:257.
[21] Sweeney J, Ward IM. J Mech Phys Solids 1996;44:1033.
[22] Bauwens-Crowet C. J Mater Sci 1973;8:968.
[23] Hope PS, Ward IM, Gibson AG. J Mater Sci 1980;15:2207.
[24] Hope PS, Duckett RA, Ward IM. J Appl Polym Sci 1980;25:1373.
[25] Macedo PB, Litovitz TA. J Chem Phys 1965;42:245.
[26] Dooling PJ, Buckley CP, Hinduja S. Polym Engng Sci 1998;38:892.
[27] Babaiikochekseraii S. MSc, University of Manchester, 1991.
[28] Adams AM, Buckley CP, Jones DP. Polymer 1998;39:5761.
[29] Buckley CP, Dooling PJ, Harding J, Ruiz C, Trojanowski A. 11th International Conference on Deformation, Yield and Fracture of Polymers. Cambridge, 2000.
[30] Ferry JD. Viscoelastic properties of polymers. 3rd ed. New York: Wiley, 1980.
[31] Kahar N, Duckett RA, Ward IM. Polymer 1978;19:136.
[32] Flory PJ. Statistical mechanics of chain molecules. Munich: Hanser Publishers, 1969.